HHS Public Access

Author manuscript

Curr Biol. Author manuscript; available in PMC 2021 June 22.

Published in final edited form as:

Curr Biol. 2020 June 22; 30(12): 2379–2385.e4. doi:10.1016/j.cub.2020.04.029.

Basal forebrain parvalbumin neurons mediate arousals from sleep induced by hypercarbia or auditory stimuli

James T. McKenna[1,*], **Stephen Thankachan**[1,*], **David S Uygun**[1], **Charu Shukla**[1], **James M. McNally**[1], **Felipe Schiffino**[1], **Joshua Cordeira**[1,4], **Fumi Katsuki**[1], **Janneke C. Zant**[1], **Mackenzie C. Gamble**[2], **Karl Deisseroth**[3], **Robert W. McCarley**[1,†], **Ritchie E. Brown**[1,#], **Robert E. Strecker**[1,#], **Radhika Basheer**[1,#,**]

[1]VA Boston Healthcare System and Harvard Medical School, Psychiatry, West Roxbury, MA 02132, USA

[2]Boston VA Research Institute, Inc., Boston, MA 02109, USA

[3]Stanford University, Psychiatry and Behavioral Sciences/Bioengineering, Stanford, CA 94305, USA

[4]Department of Biological & Environmental Sciences, Western Connecticut State University, Danbury, CT 06810 USA.

SUMMARY

The ability to rapidly arouse from sleep is important for survival. However, increased arousals in patients with sleep apnea and other disorders prevent restful sleep, and contribute to cognitive, metabolic and physiologic dysfunction [1, 2]. Little is currently known about which neural systems mediate these brief arousals, hindering the development of treatments which restore normal sleep. The basal forebrain (BF) receives inputs from many nuclei of the ascending arousal system including the brainstem parabrachial neurons which promote arousal in response to elevated blood carbon dioxide levels, as seen in sleep apnea [3]. Optical inhibition of the terminals of parabrachial neurons in the BF impairs cortical arousals to hypercarbia [4], but which BF cell types mediate cortical arousals in response to hypercarbia or other sensory stimuli is unknown. Here we tested the role of BF parvalbumin (PV) neurons in arousal using optogenetic techniques

**CORRESPONDING AUTHOR: Dr. Radhika Basheer, radhika_basheer@hms.harvard.edu.

*shared first authorship

#shared senior authorship

†deceased

AUTHORS' CONTRIBUTIONS

J.T.M., S.T., J.M.M., J.C.Z., R.E.B., R.W.M., R.E.S., and R.B. conceived and designed the experiments. S.T., J.T.M., D.S.U., C.S., J.C., J.M.M., F.S., F.K., and J.C.Z. performed the experiments. S.T., J.T.M., C.S., D.S.U., J.M.M., F.K., F.S., M.C.G., and R.B. analyzed the data; J.T.M., R.E.B., J.M.M., R.E.S., and R.B. drafted and revised the manuscript for content. Other authors provided comments on the manuscript. K.D. provided AAV-DIO-ChR2-EYFP through the UNC Vector Core.

DECLARATION OF INTERESTS

The authors declare no competing financial interests. JTM received partial salary compensation and funding from Merck MISP (Merck Investigator Sponsored Programs) but has no competing financial interest with this work. MCG received salary compensation from Merck MISP but has no competing financial interest with this work.

in mice. Optical stimulation of BF-PV neurons produced rapid transitions to wakefulness from non-rapid-eye movement (NREM) sleep but did not affect REM-wakefulness transitions. Unlike previous studies of BF glutamatergic and cholinergic neurons, arousals induced by stimulation of BF-PV neurons were brief and only slightly increased total wake time, reminiscent of clinical findings in sleep apnea [5, 6]. Bilateral optical inhibition of BF-PV neurons increased the latency to arousal produced by exposure to hypercarbia or auditory stimuli. Thus, BF-PV neurons are an important component of the brain circuitry which generates brief arousals from sleep in response to stimuli which may indicate physiological dysfunction or danger to the organism.

eTOC blurb

Brief arousals from sleep in sleep apnea and other disorders hinder the restorative effects of sleep. Using optogenetic techniques in mice, McKenna *et al.* identify basal forebrain parvalbumin neurons as an important contributor to brief arousals from sleep elicited by increased carbon dioxide levels or acoustic stimuli.

Keywords

GABAergic; parvalbumin; channelrhodopsin2; ArchT; Ascending reticular activating system; sleep apnea; basal forebrain; sleep-wake; hypercarbia; cortical arousal

RESULTS

Excitation of BF-PV neurons produces rapid and brief arousals from NREM sleep.

To test the effect of exciting BF-PV neurons, we used bilateral viral vector injections into BF to transduce them with a channelrhodopsin2 (ChR2) and enhanced yellow fluorescent protein (EYFP) fusion protein; or EGFP (non-opsin control, STAR Methods; Figure 1A)[7–9]. Immunohistochemical analysis validated the efficient and selective ChR2-EYFP transduction of BF-PV neurons. Within a 1mm × 1mm box in the BF coronal brain section with most transduction, >80 % of cells transduced with AAV-ChR2-EYFP expressed PV (N=3), confirming selectivity and ~54% of the PV neurons were transduced with ChR2-EYFP, similar to values previously reported by us and others [9, 10], indicating high efficiency. For arousal studies, at least one month after injections of viral vectors, transduced BF-PV neurons were optically stimulated bilaterally with 40 Hz trains of 10 ms light pulses (473-nm) for 5 s, followed by 55 s of no stimulation. This stimulation cycle was repeated for six hours during the light period when mice prefer to sleep (Figure 1B). The stimulation frequency of 40 Hz is within the natural discharge range of BF-PV neurons during brain activated states [9, 11], and was chosen since we previously found that this frequency of stimulation was particularly effective in activating the cortex [9]. Effects of stimulation were compared with counterbalanced recordings on a different day analyzed at the same timepoints with the laser off (Laser off condition). We additionally examined response to laser light illumination of BF in a non-opsin control group, where BF-PV neurons expressed EGFP alone.

Since stimulations were performed at regular intervals, they could occur in any behavioral state. Only stimulations occurring during NREM and REM sleep were analyzed. Analysis of

stimulations which occurred during NREM sleep revealed that the latencies to arousal (NREM→wake transitions) were significantly decreased when compared to the laser off condition. Raster plot depiction (Figure 1C) of one representative case illustrates the striking decrease in the median latency to arousal due to optogenetic stimulation of BF-PV neurons. Overall, optogenetic stimulation produced a significant (~4 fold) decrease in arousal latency (comparison of the means of the median values per animal; laser off 19.5±1.0 s vs. ChR2 Stim 4.0±0.7 s; t=12.123 (df13), P<0.001). We note that this decrease was seen in all mice tested (Figure 1D, N=14). Optical stimulation in non-opsin control mice (N=6) resulted in a median latency of 20.5±1.0 s, similar to values in the laser off condition in mice transduced with ChR2-EYFP.

These initial results demonstrated that excitation of BF-PV neurons reduced the median latency of arousals from NREM sleep. However, these data do not indicate whether this is an all-or-nothing effect or reflects a shift in the probability of a NREM-to-wake transition. Further analysis showed that ChR2 stimulation of BF-PV neurons significantly decreased the probability that the mice remained in NREM sleep following ChR2 stimulation when compared to the laser off condition (Figure 1E; 5 s bins analyzed; f=75.16 (df1), P<0.001). By the end of the 5 s stimulation period, the probability of the mouse remaining in NREM sleep dropped to 33.7±4.9 % in mice receiving bilateral ChR2 stimulation of BF-PV neurons, in contrast to 82.0±1.6 % for the laser off condition. The percentage of arousals that occurred within the 5 s of the ChR2 stimulation period was significantly elevated, when compared to the laser off condition (Figure 1F; Laser off 19.3±1.88 % vs. ChR2 Stim 67.76±4.83 %; t=−9.206 (df13), P<0.001). BF-PV stimulation therefore increased the probability of NREM-to-wake transitions, compared to the laser off condition.

Excitation of BF-PV neurons did not alter arousals from REM sleep.

Less than 10% of the stimulations occurred in REM sleep, and there was no significant difference in the latencies to arousal within 60s from start of stimulation (REM→wakefulness transitions) when compared to the laser off condition (Laser off 22.1±4.0 s vs. ChR2 Stim 19.6±3.6 s, t=1.127 (df11), p>0.284, N=12, n.s.). Very few stimulations (0–4/animal over 6 hours) that occured during REM sleep resulted in arousal within 5s of stimulation (Laser off 1.56±0.6 % vs. ChR2 Stim 0.56±0.4 %; n.s.).

Optogenetic stimulation produced a small increase in the total amount of wakefulness.

The amounts of wakefulness, NREM, and REM sleep were evaluated during the six hours of cycling (5s on; 55s off) BF-PV optogenetic stimulation (Figure 2A). Total amounts of wakefulness were significantly, but only slightly, elevated (Laser off 36.9±1.2 % of total time vs. ChR2 Stim 41.9±1.2 %; t=−4.416 (df13), P<0.001; 13.6 % increase). NREM sleep amounts were slightly but significantly decreased (Laser off 54.0±1.2 % vs. ChR2 Stim 50.1±1.7 %; t=3.411 (df13), P<0.01; 7.2% decrease), and REM sleep amounts were not significantly altered (Laser off 9.1± 0.7% vs ChR2 Stim 8.4± 0.3; t=0.832 (df13) P>0.42, n.s.). Wake bout durations over the 6 hrs of stimulation were significantly increased due to ChR2 stimulation (Figure 2B; Laser off 49.5±4.5 s vs. ChR2 Stim 59.6±5.9 s; t=−2.326 (df13), P=0.037; +20.5%), and NREM sleep bout durations exhibited a trend-level decrease (Laser off 68.3±7.1 s vs. ChR2 Stim 58.4±5.2 s; t=1.958 (df13), P=0.072; −16.2%).

Although REM sleep differences did not approach significance, we note that the −17.2% decrease in REM sleep bout durations (Laser off 71.2±9.6 s vs. ChR2 Stim 58.9±5.2 s) would be predicted to accompany this increase in wake bout durations produced by ChR2 stimulation. Blue light illumination in non-opsin EGFP control mice (N=6) did not significantly alter behavioral states (Wakefulness: Laser off 35.9±3.1 % vs. Laser on 35.8±1.2 %; NREM: Laser off 53.7±2.9 % vs. Laser on 54.4±1.7 %; REM: Laser off 10.3±0.5 % vs. Laser on 9.8+0.6 %; t tests, P>0.05, n.s.). To summarize, repeated optical stimulation of BF-PV neurons produced rapid arousals from NREM sleep, and the resultant wake bout durations were significantly increased but overall amounts of wake were only slightly elevated.

Optogenetic inhibition of BF-PV neurons inhibits arousals due to hypercarbia

In the next series of experiments, we used optogenetic inhibition with ArchT to test whether BF-PV neurons play a role in the arousals from sleep induced by two important types of stimuli which may indicate danger to the animal i.e. increased carbon dioxide levels (hypercarbia) and loud auditory stimuli (Figure 3A–C). BF-PV neurons were bilaterally transduced with ArchT-GFP and optical fibers implanted for ArchT activation (Figure 3A). Histological and immunohistochemical analysis validated ArchT-GFP transduction of BF-PV neurons (Figure 3C, Figure S1), similar to our previous studies targeting these neurons [9]. Results were compared within animal and with a control non-opsin fluorophore-only (EGFP) control group exposed to the same laser paradigm.

Mice (N=7) were placed in a chamber (Figure 3B) where they were exposed to brief (30s) elevations in the ambient level of CO_2 (1 % to 10%), cycling every 5 minutes for four hours during the light period. Alternating CO_2 exposures were coupled with bilateral optogenetic inhibition of BF-PV neurons. This inhibition consisted of 40 s of continuous green light (20mW), 10 s preceding CO_2 exposure, and continuing throughout the CO_2 exposure (30s). With exposure to CO_2 alone, latency to cortical arousal from NREM was 15.99±1.23 s (Figure 3D, E), similar to that reported by Kaur and colleagues [4, 12]. When this hypercarbia stimulus was presented while bilaterally inhibiting BF-PV neurons, the latency to arousal was markedly increased (ArchT-GFP; 25.6±1.04 s; Figure 3D, E). Mean data confirmed that latencies were significantly longer when BF-PV neurons were inhibited (Figure 3E; t=6.63 (df6), P<0.001). These changes were not seen in non-opsin EGFP control mice (Laser off 17.5±1.5 s vs. Laser on, 16.1± 1.6 s; N=7, n.s.). Probability curve analysis revealed that a greater proportion of late arousals to increasing CO_2 occurred with optical inhibition of BF-PV neurons (Figure 3F). The probability of remaining in NREM sleep in the presence of CO_2 was significantly elevated when BF-PV neurons were inhibited (f=12.19 (df1), P>0.001).

Optogenetic inhibition of BF-PV neurons inhibits arousals due to auditory stimuli

Unlike parabrachial neurons, which appear to play a preferential role in mediating arousals to hypercarbia [4, 12], the BF receives multimodal input from many arousal systems [13, 14]. Thus, we predicted that BF-PV neurons would also be involved in the arousal response to other sensory stimuli. Accordingly, in our next series of experiments, we measured latencies to arousal in response to an auditory stimulus which progressively increased in

volume from 0 to 20dB above background over a 30 s period (Figure 3G–I). Bilateral optical inhibition of BF-PV neurons was applied 10 s preceding sound stimuli exposure and continued for 30 s during stimuli exposure. This pattern was repeated every 5 minutes for four hours. Like hypercarbia stimuli, these auditory stimuli reliably induced arousals from sleep (Figure 3G). When sound stimuli were presented while bilaterally inhibiting BF-PV neurons, the latency to arousal was significantly increased (Figures 3G–I; Laser off 22.4±0.9 s vs. ArchT-GFP 27.4±1.6 s; paired t-test, t=2.6 (df6), P=0.02). These changes were not seen in non-opsin control mice (Laser off 17.1±0.4 s vs. Laser on 16.9±0.7 s; N=7, n.s.). Probability curve analysis revealed a greater proportion of late arousals to auditory stimuli with inhibition of BF-PV neurons (Figure 3I). The probability of remaining in NREM was significantly higher when optical inhibition of BF-PV neurons was applied (f=2.81 (df1), P=0.002).

ArchT inhibition of BF neurons without exposure to CO_2 or increased sound levels using the same intermittent 30 s/5 min paradigm paradoxically resulted in slightly but significantly increased wakefulness (N=5, Laser off 33.6+2.1 % vs. ArchT-GFP 37.7+2.2 %; P<0.017), possibly due to the powerful H-currents in BF PV neurons [15] which may lead to rebound excitation and arousals at the offset of ArchT-mediated hyperpolarizations. We note that this cumulative effect over the whole four hours would, if anything, tend to counteract the decreasein arousal latency we observed with ArchT inhibition during CO_2/sound exposure. Concomitantly, amounts of NREM sleep were slightly decreased (Laser off 56.4±1.8 % vs. ArchT-GFP 53.2±1.9 %, P<0.006) with no significant differences in REM sleep (laser off 10.0+0.6 % vs. ArchT-GFP 9.1+0.5, n.s.). Green laser illumination in control, non-opsin mice (N=5) had no significant effect on wakefulness (p=0.11).

DISCUSSION

In normal individuals, brief cortical arousals from sleep occur throughout the sleep period [16, 17]. The frequency of these arousals is markedly increased in sleep apnea [5], insomnia [18], and during aging [19]. Increased arousals from sleep interfere with the restorative effects of sleep [20] and have numerous deleterious consequences, including impaired synaptic plasticity and memory formation [21], disrupted cardiovascular regulation [22] and immune system dysfunction [23,24]. Here we identify BF-PV neurons as a mediator of brief arousals in response to hypercarbia or auditory stimuli.

To be effective in mediating arousal responses to important sensory stimuli, an arousal system should ideally generate a rapid cortical response, in preparation for a more prolonged period of wakefulness if the threat persists. However, to not disrupt sleep more than necessary, these arousals should be brief. Thus, in our first set of experiments, we used optogenetic techniques in mice to precisely measure the latency to arousal from sleep, as well as the overall effect on total amounts of sleep, in response to bilateral optical stimulation of BF-PV neurons. These experiments showed that NREM-to-wake arousal latencies produced by stimulation of BF-PV neurons were substantially faster than those previously reported for stimulation of cholinergic neurons (~13.5s [25]; 25–45 s [10]); or hypocretin/orexin neurons (20–40 s) [26]. In contrast, arousals from REM sleep to wakefulness were not altered by stimulation of BF-PV neurons, consistent with the high

spontaneous discharge rate of BF-PV neurons during the REM sleep state [9, 11]. BF-PV stimulations during NREM sleep led to arousals which were brief, with only a small increase in total wakefulness, similar to clinical sleep apnea data which report relatively little change in overall sleep-wake amounts despite many arousals during the night [5, 6]. These sleep-wake findings are broadly consistent with a previous study which showed that 10 Hz optogenetic stimulation of BF-PV neurons promoted wakefulness at the expense of NREM sleep, but was less effective compared to optogenetic stimulation of either glutamatergic or cholinergic BF neurons [11]. Another heavily studied subpopulation of BF GABAergic neurons, somatostatin-expressing neurons, promote sleep and are thus unlikely to play a role in rapid-arousal [11, 27]. Thus, when considering BF neurons, the PV neurons appear to play a more focused role in brief arousals from NREM sleep, compared to other BF neuronal subpopulations. Outside the BF, other neurotransmitter systems may be involved in rapid arousals from sleep in response to various physiological challenges. For example, optogenetic stimulation of noradrenergic locus coeruleus neurons (< 4s) [28] or hypothalamic neurotensin neurons (< 5s) [29] also produces rapid arousals from sleep.

Although gain-of-function experiments are informative, loss-of-function tests are more powerful in testing the role of a particular neurotransmitter system in a physiologic function. Our optogenetic inhibition experiments indicated that BF-PV neurons mediate arousals from NREM sleep produced by hypercarbia or acoustic stimuli. Recent evidence suggested that the BF is a component of the arousal system mediating arousals in response to hypercarbia [3, 4]. The BF, along with the lateral hypothalamus and the central nucleus of the amygdala, receives excitatory innervation from the wake promoting PBel (extended lateral aspect of the parabrachial nucleus) area of the brainstem, which is critically involved in arousals to CO_2, but not arousals to sounds. Optogenetic inhibition of the majority subpopulation of glutamatergic neurons in PBel, which is characterized by calcitonin gene-related peptide (CGRP) immunoreactivity, delayed latencies to arousal in response to CO_2. Interestingly, optogenetic inhibition of transduced PBel CGRP neuronal terminals in BF, LH and CeA delayed arousal latencies to CO_2, with the most profound effect observed in the BF. Here we extend this work by showing that inhibiting the subpopulation of BF neurons which contain PV attenuates arousals from NREM in response to CO_2.

In contrast to the findings of Kaur et al. (2017)[4], who found a selective role for the parabrachial nucleus in mediating arousals in response to elevated CO_2, we found that inhibition of BF PV basal forebrain neurons extended arousal latencies elicited by either CO2 *or* sound suggesting that BF PV neurons play a more universal role in sensory stimuli-induced arousal. These findings are consistent with previous work by Dringenberg and colleagues [30] who showed that inhibition of basal forebrain using lidocaine blocks cortical activation produced by electrical stimulation of the inferior colliculus, implicating the BF in cortical arousals produced by activation of the auditory system in the brainstem. We have not investigated the pathway from the brainstem to the BF in our study but based on work of others, one possibility is a medial geniculate nucleus of the thalamus-amygdala-BF relay [31]. Collectively, our results suggest that BF-PV neurons are an important component of the ascending arousal circuitry which mediates brief arousals from sleep in response to multiple stimuli indicating danger. A logical extension of this study suggests BF-PV neurons as a candidate target to therapeutic intervention of sleep apnea patients suffering with low arousal

thresholds. BF-PV neurons may also be an interesting target for treatments to prevent arousals from sleep due to ambient noise.

STAR METHODS

Lead Contact

Further information and requests for resources and reagents should be directed to and will be fulfilled by the Lead Contact, Radhika Basheer (Radhika_Basheer@hms.harvard.edu).

Materials Availability

This study did not generate new unique reagents.

Data and Code Availability

The datasets supporting the current study have not been deposited in any public repository but are available from the lead author upon request. This study did not generate new code.

Experimental Models and Subject Details

Animals.—Adult (4–6 months) homozygous PV-Cre mice (B6;129P2-*Pvalb*$^{tm1(cre)Arbr}$/J) were purchased from Jackson Laboratory (Stock#008069; Bar Harbor, Maine) and bred in house. Mice were housed at 21°C with a 12-h light/ dark cycle (7:00 AM–7:00 PM), and food and water *ad libitum*. All procedures were performed in accordance with the National Institutes of Health guidelines and in compliance with the animal protocol approved by the VA Boston Healthcare System Institutional Animal Care and Use Committee.

Method Details

Viral vector injections.—For optical excitation of BF-PV neurons we used adeno-associated viral vectors serotype 5 (AAV5), with Cre-recombinase dependent expression of a fusion protein, consisting of ChR2 and EYFP (AAV-DIO-ChR2-EYFP; 3×10^{12} viral particles/ml estimated by DotBlot, University of North Carolina Vector Core; Chapel Hill, NC). For inhibition of BF-PV neurons AAV5-CAG-flex-reverse-ArchT-GFP (hereafter referred to as AAV-FLEX-ArchT), bearing the ArchT strain Halorubrum sp. TP009, was purchased from the University of North Carolina vector core. Laser light, non-opsin fluorophore-only, control experiments used cre-dependent AAV1/2-EGFP vectors (Genedetect, Auckland, NZ). Virion concentration was estimated to be 2×10^{12} particles/ml by DotBlot. Viral vectors (500 nL for AAV-DIO-ChR2-EYFP; 1 uL for AAV-FLEX-ArchT) were bilaterally injected into the basal forebrain (BF; AP 0.0 mm, ML ± 1.6 mm, and ventral −5.0 to −5.3 mm) of PV-Cre mice under isoflurane anesthesia (induction, 5%; maintenance, 1–2%) using a Nanoliter microdispenser (Nanoliter 2010 injector, 23nl/step, slow release; World Precision Instruments; Sarasota, Fl) or a Hamilton syringe (50 nl/minute) driven by a high-precision injector pump (model 250; KD Scientific). Following the injections, the scalp incision was sutured closed and mice were allowed to recover. We previously confirmed effective optogenetic excitation and inhibition of BF-PV neurons using these vectors *in vitro* [9].

EEG/EMG electrode and fiber optic cannula implantation.—Two or more weeks following AAV viral injections, EEG screw electrodes were bilaterally implanted into the skull above the frontal cortices (AP = 1.5–1.9 mm; ML = ±1.0–1.5 mm) under isoflurane anesthesia. A reference screw was placed above the cerebellum, and electromyography (EMG) electrodes were placed in the nuchal muscle. Electrodes were connected to EEG/EMG headmounts (Pinnacle Technology Inc., part # 8402-SS, KS, USA). Fiber optical cannulae (200μm, 0.22 NA optical fiber, Doric Lenses; Quebec City, Quebec, CA) were implanted targeting BF (AP 0.0 mm, ML ±1.6 mm, and ventral 5.0 mm). The headmount and fiber optic cannulae were secured to the skull using dental cement.

In Vivo EEG/EMG recordings.—For optical excitation work, at least one week following EEG/EMG surgery, mice were tethered and acclimatized to the recording chamber for at least 4 days. After acclimatization, continuous EEG/EMG (8200-K1-SL amplifier; Pinnacle Technology or Model 3600 16-Channel Extracellular Amplifier; A-M Systems) and video recordings were performed before, during, and after optical (or laser off control) stimulation of BF-PV neurons. The EEG/EMG response to BF light stimulation was recorded using: (1) Sirenia Sleep Pro (Pinnacle Technologies); or (2) the Spike2 analysis program (Cambridge Electronic Design; Cambridge, UK) and a CED1401 analog-to-digital converter (Cambridge Electronic Design). EEG signals were sampled at 2–4 KHz and bandpass filtered at 1–200 Hz. For hypercapnia and acoustic arousal work, mice were tethered and acclimatized to the recording chamber for 4 hours (9am-1pm). After acclimatization, continuous EEG/EMG recordings (8200-K1-SL amplifier; Pinnacle Technology) with and without optical stimulation of BF-PV neurons for 4 hours (1pm–5pm). EEG/EMG and other signals were recorded with WinWCP (Strathclyde Institute of Pharmacy and Biomedical Sciences).

Optical excitation of BF-PV neurons.—Optical stimulation was performed bilaterally to excite BF-PV neurons transduced with ChR2 using a fiber-coupled 473-nm solid-state laser diode (Cat # CL473–050-O; 20 mW; CrystaLaser; Reno, Nevada) and an optical fiber (Doric Lenses) connected to the implanted fiber optic cannula with a zirconium sleeve. The non-opsin control AAV mice also were subjected to same protocol. Software-generated transistor–transistor logic (TTL) pulses were used to drive the laser light stimulation (Spike2; Cambridge Electronic Design or WinWCP; Strathclyde Institute of Pharmacy and Biomedical Sciences). 10 ms pulses were bilaterally delivered at 40 Hz for 5 s, followed by 55 s of no stimulation. This protocol was repeated for the duration of the experiments (6 hours, ZT 2–8; Figure 1B). Time-of-day matched TTL pulses alone (laser off condition) in the same mice on a different day served as control.

Sleep scoring and multi-taper analysis for optogenetic excitation experiments.—Vigilance states were scored in 4 s epochs as one of the following: (1) Wake; active behavior accompanied by desynchronized EEG (low in amplitude), and tonic/phasic motor activity evident in the EMG signal; (2) NREM sleep; more synchronized EEG, higher in amplitude, with particularly notable power in the delta (0.5–4 Hz) band, and low motor activity (EMG); and (3) REM sleep; small amplitude EEG, particularly notable power in the theta (4–9 Hz) band, muscle atonia interrupted by phasic motor activity (EMG). Compared

to wake, EEG power during REM was significantly reduced in lower delta frequencies (0.5–4 Hz) and increased in the range of theta activity (4–9 Hz).

Measurement of arousals for optogenetic excitation.—For optogenetic stimulations that occurred after at least 10 s of NREM (determined post-hoc during EEG/EMG scoring), the latency to arousal was calculated as the time from the beginning of the stimulation to the end of the last slow wave activity leading to EEG desynchronized activity within 55 s. In < 2% of cases, optogenetic stimulation failed to result in arousal within the next 55s. For such cases, the latency was more than 60 s, extending into the next stimulation period, and not included in evaluations. The median statistic was determined per animal because of the skewed, non-normal distribution of responses. Optogenetic stimulation values were compared with that of the laser off condition (TTL pulses alone). We plotted the cumulative probability distribution of remaining in NREM sleep vs. time since stimulation per cycle, averaged for all arousals per case of bilateral optogenetic stimulation (N=14), and compared to all arousals per case in the laser off condition.

Hypercapnia and auditory stimulation experiments.—Mice were recorded in custom built chambers into which CO_2 or sounds were delivered (Figure 3C). Ambient CO_2 levels were controlled using a three-channel programmable gas mixer (GSM-3; CWE Inc.) at a flow-rate of 1 L/min. CO_2 levels were continuously monitored with a cage mounted CO_2 sensor (Cozir Sprint). Auditory stimuli were generated using a custom MATLAB script and delivered via WinEDR software (University of Strathclyde, Glasgow, UK) to cage mounted speakers. Background and stimulus dB were continuously monitored using a cage mounted microphone (MAX4466; Adafruit). Both CO_2 and auditory sensor signals were fed via an Arduino Uno to a recording device (USB-6341; National Instruments). From the onset of recordings, EEG/EMG and gas or sound signals were sampled at 1kHz using WinEDR. This software was also used to control switching on/off the lasers, gas and acoustic stimuli. Activation of inhibitory ArchT was conferred by light delivered from a 532 nm laser (MGL-III-532–100mW; Opto Engine, Midvale, UT), delivered to BF via a fiberoptic patch cable (MFP_200/220/900–0.22_2m_FCM-MF1.25; Doric Lenses) into WinEDR.

Measurement of arousals for optogenetic inhibitions.—For ArchT optogenetic inhibitions that occurred after at least 10 s of NREM (determined post-hoc during EEG/EMG scoring), the latency to arousal was calculated visually from EEG records as the time from the beginning of the stimuli presentation (CO_2 infusion or sound) to the end of the last slow wave activity, indicated by EEG desynchronized activity for >2s. Muscle tone was not a necessary criterion in determining arousals. Values were compared between laser off +CO_2 vs. optogenetic ArchT BF-PV stim+CO_2 exposure; or laser off+sound stimuli vs. optogenetic ArchT BF-PV stim+sound stimuli exposure. We plotted the probability distribution of remaining in NREM sleep vs. time since the beginning of stimulation per cycle, averaged for all arousals per case of ArchT inhibition during CO_2 infusion or sound stimuli exposure (laser on), and compared to all arousals per case in the laser off condition (TTL pulse alone+CO_2 infusion or sound stimuli) exposure (N=7).

Perfusion/brain extraction.—Mice were anesthetized with sodium pentobarbital (50 mg/ml), exsanguinated with ice-cold PBS, and perfused transcardially with 10% formalin (Cat # HT5011; Sigma-Aldrich; St. Louis, MO). Brains were post-fixed for 2 days in 10% formalin and in 30% sucrose for a third day. 40 μm-thick coronal slices were collected in 1 of 4 wells (phosphate buffered saline) and stored at 4°C.

Anti-GFP/PV antibody labeling.—According to information provided by the manufacturer (RnD Systems; Minneapolis, MN), the sheep anti-PV primary antibody (Cat # AF5058) precipitated a single 12 kDa band on Western blots from rat, mouse, and human brain tissue. This antibody has been previously characterized [32,33,34]. PV labeling was similar to that previously reported in many brain regions in the mouse [9, 11, 15, 35,36] and rat [37–40], including the cortex, medial septum/vertical limb of the diagonal band, BF, and the thalamic reticular nucleus.

Tissue was first blocked with 0.5% TX-100 in PBS + 3% normal donkey serum for 1 hour. Sections were then incubated overnight in primary antibody (mouse anti-GFP; 1:1000; Cat # MAB3580; EMD Millipore; Billerica, MA) followed by 3 hours of incubation with secondary antibody (donkey anti-mouse IgG conjugated to AlexaFluor 488, green; 1:100; Cat # A-21202; ThermoFisher Scientific; Waltham, MA). This was followed by overnight incubation in the second primary antibody (sheep anti-PV; 1:200; Cat # AF5058; RnD Systems) and then next-day appropriate secondary antibody for 3 hours (donkey anti-sheep IgG conjugated to AlexaFluor 594, red; 1:100; Cat#A-11016; ThermoFisher Scientific). Control stains were performed in slices where primary antibodies were omitted. In some cases, optogenetic fiber optic cannula location was also determined employing cresyl violet staining on another well of tissue, using a previously established protocol [41].

Tissue mounting/microscopy and photography.—Fluorescently labeled sections were mounted onto gel-alum subbed slides and coverslipped using Vectashield Hard Set mounting medium (Cat # H-1400; Vector Laboratories; Burlingame, CA). Fluorescent microscopy and photography were performed using a Zeiss Image2 microscope, with a Hamamatsu Orca R2 camera (C10600). PV+ cells were identified by red somata (PV stain), co-localized with green (EYFP viral transfected, amplified with anti-GFP antibody) cytoplasm/soma. Labeled cells were quantified using Neurolucida software (Microbrightfield; Williston, VT). Optogenetic fiber optic cannula locations were mapped onto appropriate schematic templates [41] employing Adobe Illustrator (v.CS5.1). One case for BF-PV ChR2-EYFP, and one case for ArchT-GFP studies, were not evaluated due to histological complications.

Quantification and Statistical Analysis

For optogenetic stimulation experiments (ChR2 and ArchT), comparisons between optogenetic stimulation and laser off controls were performed using paired t-tests. Statistical analysis used SPSS software (release 11.5), and differences were determined to be significant when $P<0.05$. Cumulative probability distribution analysis (Figures 1E, **4D, and 5D**) was evaluated using repeated measures ANOVA, based on that previously employed [4, 12, 24]. Due to inequality of variances (failure of sphericity) found between the two

conditions in the optogenetic excitation studies (Figure 1E; ChR2 Stim vs laser off condition), data was analyzed using nparLD package in R (R Core Team, 2019) with an LD-F2 (longitudinal data; Condition stratifies Time) design, allowing a robust nonparametric analysis of longitudinal data in factorial settings [42]. Non-parametric probability was represented as the probability that Condition 1 (laser off) is larger than Condition 2 (Stim). All averaged data are presented as means ± standard error.

Supplementary Material

Refer to Web version on PubMed Central for supplementary material.

ACKNOWLEDGEMENTS

This work was supported by VA Biomedical Laboratory Research and Development Service Merit Awards I01 BX001404 (RB), I01 BX001356 & I01 BX004673 (REB), I01 BX000270 & I01 BX002774 (RES), I01 BX004500 (JMM) and VA CDAs IK2 BX002130 (JMM) and IK2 BX004905 (DSU); and NIH support from R21 NS079866 (RB), R21 NS079866 (REB), R21 NS093000 (REB), R01 MH039683 (REB), T32 HL07901 (JC, FK, DSU) and P01 HL095491 (RES). JTM received partial salary compensation and funding from Merck MISP (Merck Investigator Sponsored Programs) but has no conflict of interest with this work. JTM, JMM, DSU, RES, RWM and RB are Research Health Scientists at VA Boston Healthcare System, West Roxbury, MA. The contents of this work do not represent the views of the U.S. Department of Veterans Affairs or the United States Government.

REFERENCES

1. Durmer JS, and Dinges DF (2005). Neurocognitive consequences of sleep deprivation. Seminars in neurology 25, 117–129. [PubMed: 15798944]
2. Shamsuzzaman AS, Gersh BJ, and Somers VK (2003). Obstructive sleep apnea: implications for cardiac and vascular disease. JAMA 290, 1906–1914. [PubMed: 14532320]
3. Kaur S, and Saper CB (2019). Neural circuitry underlying waking up to hypercapnia. Frontiers in neuroscience 13, 401. [PubMed: 31080401]
4. Kaur S, Wang JL, Ferrari L, Thankachan S, Kroeger D, Venner A, Lazarus M, Wellman A, Arrigoni E, Fuller PM, et al. (2017). A genetically defined circuit for arousal from sleep during hypercapnia. Neuron 96, 1153–1167.e1155. [PubMed: 29103805]
5. Guilleminault C, Tilkian A, and Dement WC (1976). The sleep apnea syndromes. Annual review of medicine 27, 465–484.
6. Dempsey JA, Veasey SC, Morgan BJ, and O'Donnell CP (2010). Pathophysiology of sleep apnea. Physiological reviews 90, 47–112. [PubMed: 20086074]
7. Sohal VS, Zhang F, Yizhar O, and Deisseroth K (2009). Parvalbumin neurons and gamma rhythms enhance cortical circuit performance. Nature 459, 698–702. [PubMed: 19396159]
8. Cardin JA, Carlen M, Meletis K, Knoblich U, Zhang F, Deisseroth K, Tsai LH, and Moore CI (2009). Driving fast-spiking cells induces gamma rhythm and controls sensory responses. Nature 459, 663–667. [PubMed: 19396156]
9. Kim T, Thankachan S, McKenna JT, McNally JM, Yang C, Choi JH, Chen L, Kocsis B, Deisseroth K, Strecker RE, et al. (2015). Cortically projecting basal forebrain parvalbumin neurons regulate cortical gamma band oscillations. Proceedings of the National Academy of Sciences of the United States of America 112, 3535–3540. [PubMed: 25733878]
10. Irmak SO, and de Lecea L (2014). Basal forebrain cholinergic modulation of sleep transitions. Sleep 37, 1941–1951. [PubMed: 25325504]
11. Xu M, Chung S, Zhang S, Zhong P, Ma C, Chang WC, Weissbourd B, Sakai N, Luo L, Nishino S, et al. (2015). Basal forebrain circuit for sleep-wake control. Nat Neurosci 18, 1641–1647. [PubMed: 26457552]
12. Kaur S, Pedersen NP, Yokota S, Hur EE, Fuller PM, Lazarus M, Chamberlin NL, and Saper CB (2013). Glutamatergic signaling from the parabrachial nucleus plays a critical role in hypercapnic

arousal. The Journal of neuroscience : the official journal of the Society for Neuroscience 33, 7627–7640.

13. Brown RE, Basheer R, McKenna JT, Strecker RE, and McCarley RW (2012). Control of sleep and wakefulness. Physiological reviews 92, 1087–1187. [PubMed: 22811426]
14. Zaborszky L, van den Pol A, Gyengesi E, (2012). The basal forebrain cholinergic projection system in mice, (Academic Press).
15. McKenna JT, Yang C, Franciosi S, Winston S, Abarr KK, Rigby MS, Yanagawa Y, McCarley RW, and Brown RE (2013). Distribution and intrinsic membrane properties of basal forebrain GABAergic and parvalbumin neurons in the mouse. The Journal of comparative neurology 521, 1225–1250. [PubMed: 23254904]
16. Halasz P (2004). The microstructure of sleep: Supplements to clinical neurophysiology 57, 521–533. [PubMed: 16106653]
17. Prerau MJ, Brown RE, Bianchi MT, Ellenbogen JM, and Purdon PL (2017). Sleep neurophysiological dynamics through the lens of multitaper spectral analysis. Physiology (Bethesda) 32, 60–92. [PubMed: 27927806]
18. Wei Y, Colombo MA, Ramautar JR, Blanken TF, van der Werf YD, Spiegelhalder K, Feige B, Riemann D, and Van Someren EJW (2017). Sleep stage transition dynamics reveal specific stage 2 vulnerability in insomnia. Sleep 40(9) doi: 10.1093/sleep/zsx117.
19. Li J, Vitiello MV, and Gooneratne NS (2018). Sleep in normal aging. Sleep medicine clinics 13, 1–11. [PubMed: 29412976]
20. McKenna JT, Tartar JL, Ward CP, Thakkar MM, Cordeira JW, McCarley RW, and Strecker RE (2007). Sleep fragmentation elevates behavioral, electrographic and neurochemical measures of sleepiness. Neuroscience 146, 1462–1473. [PubMed: 17442498]
21. Tartar JL, Ward CP, McKenna JT, Thakkar M, Arrigoni E, McCarley RW, Brown RE, and Strecker RE (2006). Hippocampal synaptic plasticity and spatial learning are impaired in a rat model of sleep fragmentation. The European Journal of neuroscience 23, 2739–2748. [PubMed: 16817877]
22. Somers VK, White DP, Amin R, Abraham WT, Costa F, Culebras A, Daniels S, Floras JS, Hunt CE, Olson LJ, et al. (2008). Sleep apnea and cardiovascular disease: an American Heart Association/American College of Cardiology Foundation Scientific Statement from the American Heart Association Council for High Blood Pressure Research Professional Education Committee, Council on Clinical Cardiology, Stroke Council, and Council on Cardiovascular Nursing. Journal of the American College of Cardiology 52, 686–717. [PubMed: 18702977]
23. Luyster FS, Strollo PJ Jr., Zee PC, and Walsh JK (2012). Sleep: a health imperative. Sleep 35, 727–734. [PubMed: 22654183]
24. Besedovsky L, Lange T, and Haack M (2019). The sleep-immune crosstalk in health and disease. Physiological reviews 99, 1325–1380. [PubMed: 30920354]
25. Zant JC, Kim T, Prokai L, Szarka S, McNally J, McKenna JT, Shukla C, Yang C, Kalinchuk AV, McCarley RW, et al. (2016). Cholinergic neurons in the basal forebrain promote wakefulness by actions on neighboring non-cholinergic neurons: an opto-dialysis study. The Journal of neuroscience : the official journal of the Society for Neuroscience 36, 2057–2067.
26. Carter ME, Brill J, Bonnavion P, Huguenard JR, Huerta R, and de Lecea L (2012). Mechanism for Hypocretin-mediated sleep-to-wake transitions. Proceedings of the National Academy of Sciences of the United States of America 109, E2635–2644. [PubMed: 22955882]
27. Anaclet C, Pedersen NP, Ferrari LL, Venner A, Bass CE, Arrigoni E, and Fuller PM (2015). Basal forebrain control of wakefulness and cortical rhythms. Nat Commun 6, 8744. [PubMed: 26524973]
28. Carter ME, Yizhar O, Chikahisa S, Nguyen H, Adamantidis A, Nishino S, Deisseroth K, and de Lecea L (2010). Tuning arousal with optogenetic modulation of locus coeruleus neurons. Nat Neurosci 13, 1526–1533. [PubMed: 21037585]
29. Naganuma F, Kroeger D, Bandaru SS, Absi G, Madara JC, and Vetrivelan R (2019). Lateral hypothalamic neurotensin neurons promote arousal and hyperthermia. PLoS biology 17, e3000172. [PubMed: 30893297]

30. Dringenberg HC, Sparling JS, Frazer J, and Murdoch J (2006). Generalized cortex activation by the auditory midbrain: Mediation by acetylcholine and subcortical relays. Experimental brain research 174, 114–123. [PubMed: 16575576]

31. Chavez C, and Zaborszky L (2017). Basal forebrain cholinergic-auditory cortical network: primary versus nonprimary auditory cortical areas. Cerebral cortex (New York, N.Y. : 1991) 27, 2335–2347.

32. Stephany CE, Ikrar T, Nguyen C, Xu X, and McGee AW (2016). Nogo receptor 1 confines a disinhibitory microcircuit to the critical period in visual cortex. The Journal of neuroscience : the official journal of the Society for Neuroscience 36, 11006–11012.

33. Iijima T, Iijima Y, Witte H, Scheiffele P (2014). Neuronal cell type-specific alternative splicing is regulated by the KH domain protein SLM1. Journal of Cell Biology 3, 331–42.

34. Usoskin D, Furlan A, Islam S, Abdo H, Lönnerberg P, Lou D, Hjerling-Leffler J, Haeggström J, Kharchenko O, Kharchenko PV, Linnarsson S, Ernfors P (2015). Unbiased classification of sensory neuron types by large-scale single-cell RNA sequencing. Nat Neurosci. 18,145–53. [PubMed: 25420068]

35. Tamamaki N, Yanagawa Y, Tomioka R, Miyazaki J, Obata K, and Kaneko T (2003). Green fluorescent protein expression and colocalization with calretinin, parvalbumin, and somatostatin in the GAD67-GFP knock-in mouse. The Journal of comparative neurology 467, 60–79. [PubMed: 14574680]

36. Kim A, Latchoumane C, Lee S, Kim GB, Cheong E, Augustine GJ, and Shin HS (2012). Optogenetically induced sleep spindle rhythms alter sleep architectures in mice. Proceedings of the National Academy of Sciences of the United States of America 109, 20673–20678. [PubMed: 23169668]

37. Endo T, and Onaya T (1988). Immunohistochemical localization of parvalbumin in rat and monkey autonomic ganglia. Journal of neurocytology 17, 73–77. [PubMed: 3047326]

38. Duque A, Balatoni B, Detari L, and Zaborszky L (2000). EEG correlation of the discharge properties of identified neurons in the basal forebrain. Journal of neurophysiology 84, 1627–1635. [PubMed: 10980032]

39. Gritti I, Manns ID, Mainville L, and Jones BE (2003). Parvalbumin, calbindin, or calretinin in cortically projecting and GABAergic, cholinergic, or glutamatergic basal forebrain neurons of the rat. The Journal of comparative neurology 458, 11–31. [PubMed: 12577320]

40. Deurveilher S, Lo H, Murphy JA, Burns J, and Semba K (2006). Differential c-Fos immunoreactivity in arousal-promoting cell groups following systemic administration of caffeine in rats. The Journal of comparative neurology 498, 667–689. [PubMed: 16917819]

41. Franklin KBJ, and Paxinos G (2008). The mouse brain in stereotaxic coordinates, (Amsterdan: Elsevier Academic Press).

42. Noguchi K, Gel YR, Brunner E, Konietschke F (2012). nparLD: an R software package for the nonparametric analysis of longitudinal data in factorial experiments. Journal Stat Software. 50, 1–23.

Highlights

- Optical stimulation of basal forebrain parvalbumin neurons caused rapid arousals
- Arousals induced by stimulation of basal forebrain parvalbumin neurons were brief
- Optical inhibition suppressed arousals in response to increased carbon dioxide
- Optical inhibition suppressed arousals elicited by auditory stimuli

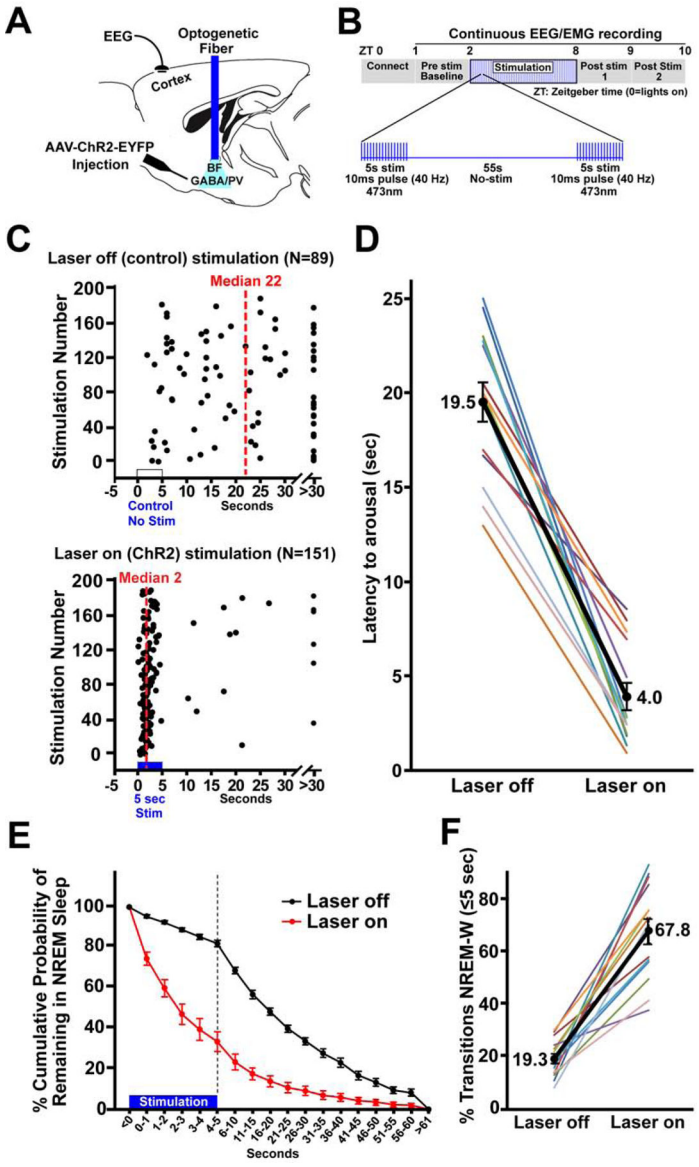

Figure 1. Bilateral optogenetic excitation of basal forebrain parvalbumin (BF-PV) neurons strongly reduced the latency to arousal from non-REM sleep.

(A) Schematic of the experiment. Adeno-associated viral vectors with Cre-dependent expression of channelrhodopsin2-enhanced yellow fluorescent proteins (AAV-DIO-ChR2-EYFP) were bilaterally injected into the BF of PV-cre mice and blue laser light applied through an implanted optical fiber to excite BF-PV neurons. An electroencephalogram (EEG) electrode implanted above frontal cortex and an electromyogram electrode in the nuchal muscle (not shown) were used to assess behavioral state.

(B) Diagram illustrating the optogenetic stimulation protocol. 40 Hz stimuli with a 10 ms pulse duration were applied simultaneously to both sides of BF for 5 s, followed by 55 s of no stimulation, repeated for 6 hours (ZT2–8).

(C) Representative raster plots for one mouse illustrate a profound decrease in the latency for arousal from NREM sleep when stimulation was applied for 6 hours (ZT2–8).

(D) Group data for all mice show that optogenetic ChR2 stimulation produced a significant decrease (~4 fold) in median NREM-Wake latencies when compared to the laser off condition in the same mice (N=14).

(E) The cumulative probability distribution of NREM-to-wake transition latencies shows an increased probability for mice to be in wakefulness when given ChR2 stimulation compared to within animal, laser off control recordings. The probability of mice remaining in NREM sleep 5 s after the start of stimulation was 33.7%, in contrast to a probability of 82.0% at the same time point in control (laser off). The first 5 s are depicted per second, to demonstrate NREM probability distribution during ChR2 stimulation. 5 s bins are then depicted for the following 55 s.

(F) When considering all arousals, the majority (67.8%) of events occurred within 5 s when mice received bilateral stimulation of BF-PV neurons, whereas in controls only 19.3% of arousals occurred within 5 s; i.e the majority of NREM-to-Wake transitions (arousals) occurred within 5 seconds from the start of bilateral BF-PV optical stimulation.

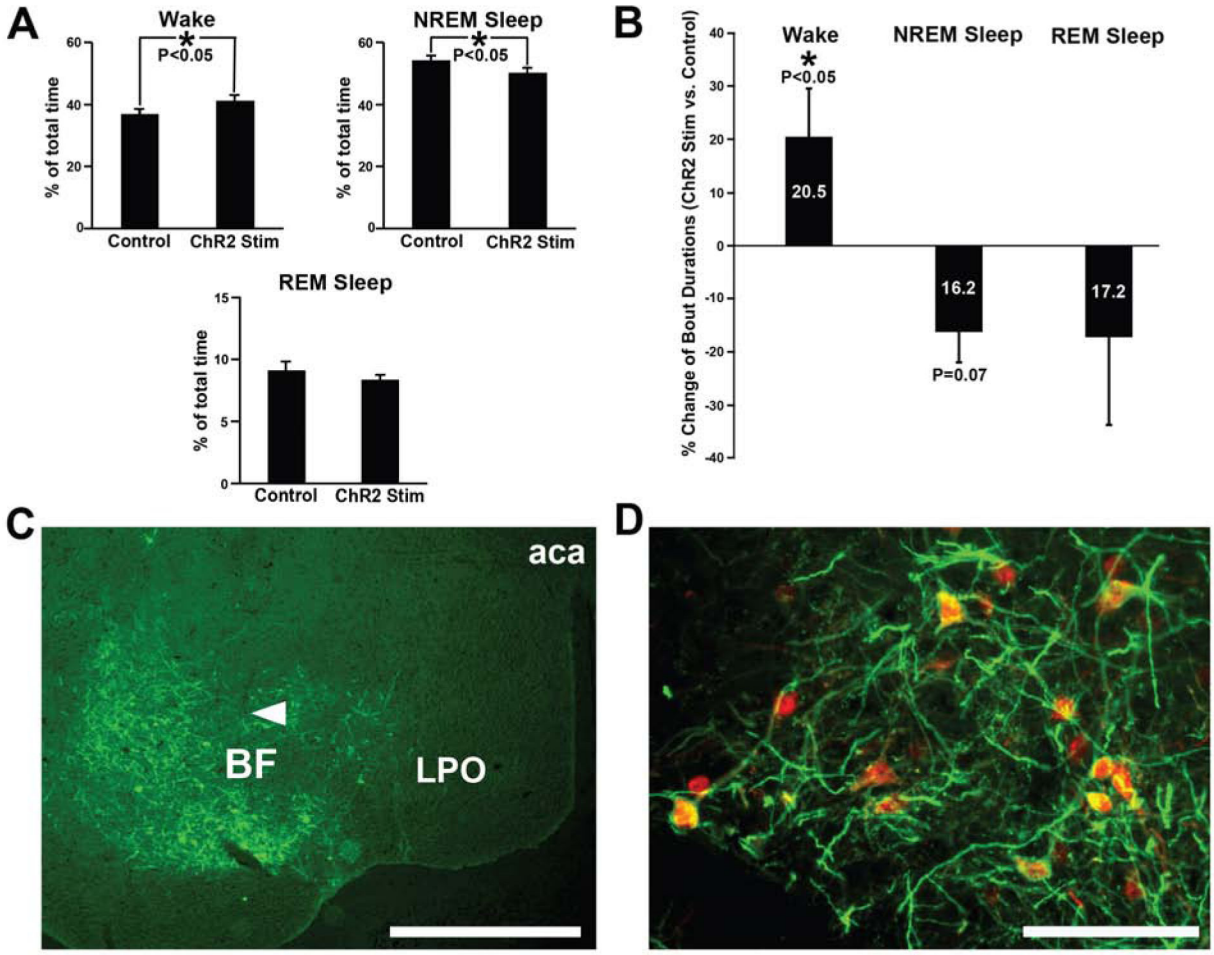

Figure 2. Bilateral optogenetic excitation of BF-PV neurons caused a small but significant increase in the overall amounts of wakefulness and decreased NREM sleep, with successful AAV-ChR2-EYFP transduction and optogenetic probe location verified.

(A) During the optical stimulation period, total amounts of wakefulness were slightly elevated, whereas NREM sleep amounts decreased, compared to laser off (no stimulation) control values. REM sleep was not significantly affected.

(B) Average wake bout durations were significantly increased (+20.5%), and NREM sleep bout duration showed a trend-level decrease (−16.2%), during the stimulation period, compared to control (laser off) stimulation. REM sleep bout durations were highly variable and not significant but tended to decrease (−17.2%).

(C) Transduction was evident throughout the majority of BF in all cases targeted for optogenetic stimulation. AAV-ChR2-EYFP injections transduced neurons and fibers throughout large areas of BF. One representative case is depicted here, and a summary of the location of the histologically confirmed location of the optical fibers is provided in Figure S1. Arrowhead denotes approximate location of the ventral tip of the fiber optic cannula, where blue light stimulation was applied. Scale bar = 1 mm. Abbreviations: aca, anterior aspect of the anterior commissure; BF, basal forebrain; LPO, lateral preoptic nucleus.

(D) Transduced neurons were PV-positive, as previously reported [9] Anti-PV immunohistochemistry (red) shows AAV-ChR2-EYFP injections (amplified with anti-GFP

primary antibody; green) selectively transduced PV somata in BF (yellow/orange). As previously reported by our group [9] , >80% of transduced neurons stained positively for PV. Scale bar = 100 μm.

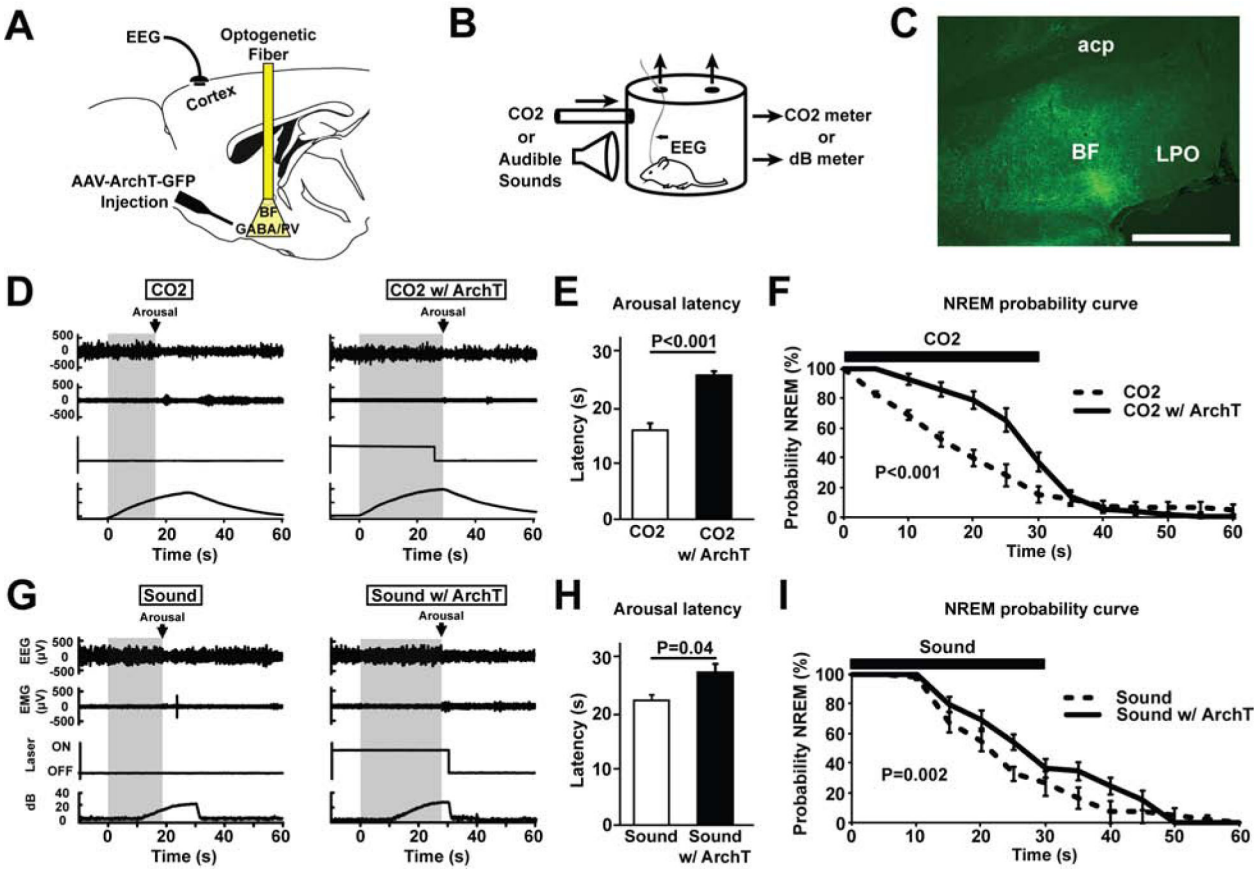

Figure 3. Bilateral optogenetic inhibition of BF-PV neurons increases the latency to arousal in response to hypercarbia (excessive CO_2) or auditory stimuli.

(A) Adeno-associated viral vectors with Cre-dependent expression of ArchT-green fluorescent proteins (AAV-Flex-ArchT-GFP) were bilaterally injected into the BF of PV-cre mice. Following transduction, green (532 nm) laser light was applied bilaterally to excite ArchT and inhibit BF-PV neurons.

(B) Mice were placed in a recording chamber where they were briefly exposed to increased CO_2 or sound levels for 30 s every 5 min.

(C) AAV-ArchT-GFP injections transduced neurons and fibers throughout large areas of BF. One representative case is depicted here. Scale bar = 1 mm. A summary of all cases in provided in Figure S1.

(D) Representative primary traces of EEG, EMG, laser on/off, and ambient CO_2 percentage levels. Left: The grey shaded area shows arousal latency from the start of the stimulus to the point at which the animal awakens, determined as the onset of desynchronized EEG lasting > 2 seconds, in response to increased CO_2. Right: In the same mouse, the latency to arousal in response to increased CO_2 was prolonged when BF-PV neurons were inhibited (CO_2 w/ ArchT), as indicated by the wider grey shaded area.

(E) Mean latencies to arouse from CO_2 (N=7) significantly differed, comparing CO_2 vs. CO_2 w/ArchT (BF-PV inhibition).

(F) NREM probability curve plots indicate that the probability that animals stay in NREM sleep during CO_2 infusion is significantly increased due to BF-PV optogenetic inhibition

(CO_2 w/ArchT), compared to the laser off condition (CO_2) or laser on, fluorophore-only controls (not shown, see main text).

(**G**) Representative primary traces of EEG, EMG, laser on/off, and ambient sounds levels. Left: The grey shaded area shows arousal latency from the start of the stimulus to the point at which the animal awakens, determined as the onset of desynchronized EEG lasting > 2 seconds, in response to increased background sound levels. Right: In the same mouse, the latency to arousal in response to increased sound was prolonged when BF-PV neurons were inhibited (CO2 w/ ArchT), as indicated by the wider grey shaded area. Note: The first 10 secs of sound stimuli were not detectable by the microphone above the background noise.

(H) Mean latencies to arouse in response to increased sound (N=7) significantly differed, comparing sound vs. sound w/ ArchT (BF-PV inhibition).

(I) NREM probability curve plots indicate that the probability that animals stay in NREM sleep during increased sound is significantly increased due to BF-PV optogenetic inhibition (sound w/ArchT), compared to the Laser off condition (sound) or Laser on, fluorophore-only controls (not shown, see main text)

Key Resources Table

Reagent or Resource	Source	Identifier
Experimental Animals		
PV-Cre mice (B6:129P2-Pvalb$^{tm1/(cre)Arbr}$/J)	Jackson Laboratory, Maine	Cat # 008069
AAV-Viral vectors		
AAV5-DIO-ChR2-EYFP	UNC Vector Core, Chapel Hill NC	N/A
AAV5-CAG-flex-reverse-ArchT-GFP	UNC Vector Core, Chapel Hill NC	N/A
AAV1/2-EGFP	Genedetect, Auckland, NZ	N/A
Antibodies		
Sheep anti-PV antibody	RnD Systems Minneapolis, MN	Cat #AF5058
Mouse anti-GFP	MilliporeSigma, Burlington, MA	Cat #MAB3580
Donkey anti-mouse IgG-AF488	ThermoFisher Scientific, Waltham, MA	Cat# A-21202
Donkey anti-sheep IgG-AF594	ThermoFisher Scientific, Waltham, MA	Cat# A-11016
Commercial Assay		
Vectashield Hardset Mounting Medium	Vector Laboratories, Burlingame, CA	CA#H-1400
Software and algorithms		
Sirenia Sleep Pro	Pinnacle Technology Inc., Lawrence, KS	N/A
Spike2 analysis program	Cambridge Electronic Design Ltd., Cambridge, UK	N/A
Illustrator (CS5.1)	Adobe, San Jose, CA	N/A
Matlab	Mathworks, Natick, MA	N/A
Neurolucida	Microbrightfield, Williston, VT	N/A
SPSS statistical software (11.5)	IBM, Armonk, NY	N/A
nparLD package in R	R Core Team, 2019	[42]